# Long term trends in aerosol optical characteristics in the Po Valley (IT)

J.P. Putaud, F. Cavalli, S. Martins dos Santos, and A. Dell'Acqua.
European Commission, Joint Research Centre (JRC), Institute for Environment and Sustainability (IES), Air and Climate Unit, Via E. Fermi 2749, 21027 Ispra VA, Italy

*Abstract*

Aerosol properties have been monitored by ground-based *in-situ* and remote sensing measurements at the station for atmospheric research located in Ispra on the edge of the Po Valley for almost one decade. *In-situ* measurements are performed according to Global Atmosphere Watch recommendations, and quality is assured through the participation in regular inter-laboratory comparisons. Sun photometer data are produced by AERONET. Data show significant decreasing trends over 2004 – 2010 for a number of variables including particulate matter (PM) mass concentration, aerosol scattering, backscattering and absorption coefficients, and aerosol optical thickness (AOT). *In-situ* measurement data show no significant trend in the aerosol backscatter ratio, but a significant decreasing trend of about -0.7 ± 0.3% $yr^{-1}$ in the aerosol single scattering albedo (SSA) in the visible light range. Similar trends are observed in the SSA retrieved from sun photometer measurements. Correlations appear between *in-situ* PM mass concentration and aerosol scattering coefficient on the one hand, and elemental carbon (EC) and aerosol absorption coefficient on the other hand, however, no increase in the EC/PM ratio was observed, which could have explained the decrease in SSA. The application of a simple approximation to calculate the direct radiative forcing by aerosols suggests a significant diminution in their cooling effect, mainly due to the decrease in AOT. Applying the methodology we present to those sites where the necessary suite of measurements is available would provide important information to inform future policies for air quality enhancement and fast climate change mitigation.

## 1- Introduction

Air-suspended particulate matter (PM) affects more people than any other pollutant worldwide (WHO), and the recognition of the relationship between PM concentrations and health outcomes (increased mortality or morbidity) has led authorities to establish limit values for $PM_{10}$ and $PM_{2.5}$ (mass concentrations of particles with an aerodynamic diameter smaller than 10 and 2.5 μm, respectively) in ambient air in many countries around the world. As a consequence, measures were

taken to reduce emissions of PM and PM precursors from various sources and PM concentrations have already decreased in several regions across the world (e.g. Begum et al., 2008, Murphy et al., 2011; Tørseth et al., 2012). Health improvements should therefore be expected.

Airborne particles however also have an impact on climate through several mechanisms, among which is direct aerosol radiative forcing resulting from the scattering, backscattering and absorption of sunlight (IPCC, 2007, and references therein). On the global scale, aerosols are estimated to cool the Earth system (e.g. Chen et al., 2011; Oh et al., 2013). A recent study showed that applying maximum feasible reduction air pollution abatement strategies would lead to a fast additional global warming of + 1.0°C by 2030, on top of the +1.2°C due to the increase of long-lived greenhouse gas concentrations (Kloster et al., 2010). Fast warming should be as far as possible avoided since adaptation to fast changes is particularly difficult (see e.g. Shaw and Etterson, 2012).

In this paper, we present ground-based remote sensing and *in-situ* aerosol data obtained over 2004-2010 at the station for atmospheric research located in Ispra (IPR), Italy. We discuss the trends observed in $PM_{2.5}$ mass concentration, aerosol scattering, backscattering and absorption coefficients, aerosol optical thickness, and intensive* variables (aerosol backscatter ratio and single scattering albedo) calculated from these measurements. These data were not included in the recent article by Collaud Coen et al. (2013) dealing with decadal trends of *in-situ* aerosol optical properties, because the data series from IPR are still less than 10 years long. However, the consistency between independent remote sensing and *in-situ* data at IPR lend robustness to the observed trends. We estimate their impact on the direct radiative forcing by aerosols and discuss how the application of our methodology to similar datasets obtained across the world would lead to important information regarding the impact of current air quality policies on changes in aerosol direct radiative forcing.

## 2- Experimental

* intensive variables are independent from the aerosol concentration, while extensive variables are proportional to the amount of particles

The station for atmospheric research of the European Commission – Joint Research Centre of Ispra (IPR) is located in a semi-rural area (45°49'N, 8°38'E, 209 m a.s.l.), on the edge of the Po valley, one of the most polluted regions in the world (see e.g. van Donkelaar et al., 2010). It sits several tens of km away from large pollution sources.

Full chemical, physical and optical characterisation of aerosols started gradually between January 2000 and November 2003. $PM_{2.5}$ gravimetric analyses are performed from quartz fiber filters collected daily according to the reference method EN19027 with two important modifications: a carbon monolith denuder is used to minimize the sampling artifacts for organic carbon, and samples are weighed at 20 ± 5% relative humidity (RH) to limit the contribution of water to the aerosol mass. $PM_{2.5}$ chemical analyses are performed following the recommendations of the co-operative program for monitoring and evaluation of the long-range transmission of air pollutants in Europe (EMEP). Organic carbon (OC) and elemental carbon (EC) are determined using the EUSAAR_2 protocol (Cavalli et al., 2010). Aerosol optical properties are measured according to the recommendations of the Global Atmosphere Watch program of the World Meteorological Organisation, and special requirements from the European Research Infrastructure projects EUSAAR (www.eusaar.net) and ACTRIS (www.actris.net). All aerosol physics instruments sample isokineticaly from a manifold equipped with a $PM_{10}$ inlet operated at ambient RH. They are described in Adam et al. (2012). Briefly, the aerosol scattering and backscatter coefficients are measured with an integrating nephelometer (TSI 3563) at 450, 550 and 700 nm, and data are corrected for angular non-idealities and truncation errors according to Anderson and Ogren (1998). The aerosol absorption coefficients at 450, 550 and 700 nm are derived from 7-wavelength Aethalometer (Magee AE31) measurements. Absorption coefficients are calculated, using a scheme based on Weingartner et al. (2003), and correction coefficients $C_0$= 3.60, 3.65, and 3.95 for 470, 520, and 660 nm, respectively. The absorption coefficients calculated for these wavelengths are interpolated to 450, 550, and 700 nm, respectively, using the observed wavelength dependence of the light absorption. The aerosol absorption coefficient at 660 nm compares very well (slope = 0.97, $R^2$ = 0.94 over 2008) with the aerosol absorption coefficient at 670 nm measured with a Multi Angle Absorption Photometer (MAAP) (Putaud, 2012). The MAAP itself was recently shown to "compare excellently with

the photoacoustic reference" instrument (Müller et al., 2011). The instrumentation took part in all the inter-laboratory comparisons organized in the frame of EMEP, EUSAAR and ACTRIS in 2006-2010, and IPR station was favorably audited by the World Calibration Centre for Aerosol Physics (WCCAP) in March 2010.

Sample flows are dried with Nafion dryers before entering instruments. However, the RH at the instrument inlets sometimes exceeds the recommended value of 40% during summer. Scattering, backscattering, and absorption data were therefore subsequently corrected for hygroscopic growth using monthly diurnal cycles of their enhancement factors as established from hygroscopic tandem diffusion mobility analyzer (HTDMA) measurements and extensively discussed in Adam et al. (2012). In brief, the particle hygroscopic growth factor $GF(\mathrm{RH})$ at any relative humidity $RH$ is estimated from $GF(90)$ assuming that $GF(RH) = (1 - RH)^{-\gamma}$. This "γ law" allows us to calculate the particle diameter in e.g. dry conditions. Assuming that particles are spherical, the volume of water in particles at instrumental RH is obtained as the difference between the particle volume at instrumental RH and at 0% RH. On the other hand, the aerosol refractive index at instrumental RH is retrieved by minimizing the difference between the aerosol scattering and absorption coefficients derived from measurements and computed from the Mie theory, and expressed as the refractive index of a mixture of dry aerosol and water. The refractive index and the number size distribution of the dry aerosol are then used to compute the optical properties of the dry aerosol. The corrections for the aerosol hygroscopic growth in the nephelometer are highest in the summer months, but generally remain marginal (median = -8%, 90$^{th}$ percentile = -23%). For the absorption coefficient, they are even smaller (median = -1%, 90$^{th}$ percentile = -3%), because absorption is much less sensitive to particle diameters than scattering. As a consequence, the correction of the aerosol scattering and absorption coefficients from instrumental to dry conditions (0% RH) results in marginal changes in SSA (median -2%, 90$^{th}$ percentile -4%).

All *in-situ* aerosol data from IPR can be retrieved from the EBAS data bank (*http://ebas.nilu.no/*).

Level 2.0 data retrieved from sun photometer measurements were taken from the AERONET web site (www.aeronet.net) without further processing, except for the interpolation to suitable wavelengths, based on the Ångström exponents obtained from the sun photometer measurements themselves.

## 3- Results and discussion

As in Collaud Coen et al. (2013), long-term trends were studied according to Weatherhead's approach (Weatherhead et al., 1998) by fitting with a least mean square approximation monthly averages of aerosol characteristics (or their logarithms) to analytical functions like:

$$Y(t) = A + Bt + \sum_{k=1}^{3} (C_k \cos(2k\pi \cdot t/12) + D_k \sin(2k\pi \cdot t/12)) + E(t) \quad (1)$$

where t is time (in months) starting from January 2004, A is a constant, B is the slope of the trend, $C_k$ and $D_k$ (k = 1, 2, 3) are the parameters describing seasonal variations in the experimental data and E(t) is the residual noise, which is plotted in Figures 1 to 6. According to a commonly adopted rule (see Collaud Coen et al., 2013, and references therein), trends are significant at the 95% confidence level when the slope B is greater than twice its standard deviation $\sigma_B$.

As none of the aerosol extensive variables we monitor is normally distributed, but closer to lognormal distributed, logarithm of the extensive variable monthly averages were considered for trend analyses. In contrast, least mean squares fits were applied directly to monthly averages of aerosol intensive variables, since their distributions are closer to normal. No autocorrelation in the noise E(t) was observed for most of the variables we studied: the correlation coefficient $R^2$ of the linear regressions between E(t) and E(t-1) is less than 0.05 for all data but the aerosol single scattering albedo derived from sun photometer measurements, and the ratio aerosol absorption coefficient / elemental carbon ($R^2 \approx 0.15 - 0.16$) .

### 3.1. Aerosol extensive variables

#### 3.1.1. Ground level characteristics

$PM_{2.5}$ monthly averages calculated from daily gravimetric analyses at 20% RH show an obvious seasonal cycle (Figure 1), with maxima in winter and minima in summer. This is mainly due to meteorology (less horizontal and vertical pollutant dispersion in winter due to a higher frequency of stagnant conditions and temperature inversions), which strongly influences the shape of the aerosol vertical profiles at IPR (Barnaba et al., 2010). The significant decreasing trend in $\log(PM_{2.5})$ ($-3.3 \pm 0.4$ % $yr^{-1}$) corresponds to a decrease in $PM_{2.5}$ of about -10% $yr^{-1}$.

A comparable seasonal cycle is observed for all other aerosol extensive variables measured at the ground. Monthly averages of the total aerosol scattering coefficient at 550 nm at instrument RH (circles) and at 0% RH (squares) are shown in Figure 2. A significant decreasing trend (-2.8 ± 0.5 % $yr^{-1}$) is observed in the logarithm of the aerosol scattering coefficient at 0% RH too. Variations of the aerosol scattering at 450 and 700 nm are very similar to those of the scattering at 550 nm.

Seasonal and inter-annual variations are also observed for the aerosol backscattering coefficient at all 3 wavelengths (not shown), with very similar patterns compared to that of the aerosol total scattering coefficient.

Monthly averages of the aerosol absorption coefficient at 520 nm (Figure 3) show a similar seasonal trend to aerosol mass concentration and scattering coefficients (maxima in winter, minima in summer). The slope of the trend in the logarithm of the aerosol absorption coefficient at 520 nm (-1.1 ± 0.3% $yr^{-1}$) is not as steep as for scattering, but still significant. The same applies to the aerosol absorption coefficients at 470 and 660 nm, which show similar seasonal and long-term variations.

3.1.2. Variables derived from sun photometer measurements

The variations in the AOT measured from Ispra at 440 nm (Figure 4) and 675 nm show clear seasonal variations with maxima generally observed from March to October. Seasonal median values of the AOT at 440 nm are 0.20, 0.34, 0.39, and 0.25 for winter, spring, summer, and autumn, respectively. Possible explanations for this include increased production of secondary aerosol, and enhanced transport of pollution plumes from the Po Valley (mountain breeze) during warm months. The trends in the logarithm of AOT are only just significant over the 2004 – 2010 period, with negative slopes (± standard errors) of -4.0 ± 1.8 % $yr^{-1}$ and -2.5 ± 1.3 % $yr^{-1}$ at 440 and 675 nm, respectively.

The aerosol absorption optical thickness (AAOT) was also derived from the sun photometer measurements performed from Ispra between Feb. 2004 and Apr. 2010. Much less clear seasonal variations are observed in AAOT compared to AOT, and the slopes of the long-term trends (not shown) are not significant (+1.0 ± 1.0 % $yr^{-1}$ and +1.2 ± 0.9% $yr^{-1}$ at 440 nm and 675 nm, respectively.

3.2. Aerosol intensive variables

3.2.1. Ground level data

The aerosol backscatter ratio (defined as the ratio between the truncation-corrected aerosol backscattering coefficient and the truncation-corrected aerosol total scattering coefficient) at 550 nm (corrected to dry conditions or not) does not show any significant trend (-0.1 ± 0.3% $yr^{-1}$) over the 2004-2010 period (Fig. 5). This is consistent with the absence of significant increase (+0.1 ± 0.4% $yr^{-1}$) of the aerosol scattering Ångström exponent between 440 and 700 nm (not shown). The absence of significant trends for both the backscatter ratio and the Ångström exponent suggests no consistent change in the mean diameter of the 100-600 nm particles, the main scatterers of visible light at IPR.

Monthly averages of the aerosol SSA at the wavelength of 550 nm (at both instrument and 0% RH) are shown on Figure 6. Significant decreasing trends in the aerosol SSA are observed, with slopes equal to -0.7 ± 0.2 % $yr^{-1}$, -0.6 ± 0.2 % $yr^{-1}$, and -0.7 ± 0.3 % $yr^{-1}$ at 450, 550, and 700 nm, respectively. These slopes are not affected by the correction of aerosol scattering and absorption coefficients from instrumental to dry conditions (0% RH).

Since they do not directly depend on aerosol concentration, intensive characteristics are much less variable than extensive properties, which renders long time trends quite robust. Furthermore, considering random uncertainties of 10% and 30% for the aerosol scattering and absorption coefficients, respectively (based on evaluations of our instruments at the WCCAP, and uncertainties related to data conversion to 0% RH), the uncertainty of the aerosol SSA estimated from the law of propagation of errors is 8% only for the median SSA value.

3.2.2. Aerosol single scattering albedo derived from sun photometer measurements

Level 2.0 aerosol SSA data at 440 and 675 nm derived from sun photometer measurements performed at IPR could be obtained from AERONET for the period Feb. 2004 – April 2010. Level 2.0 SSA data are available for episodes where $AOT_{440} \geq 0.4$ only, and according to Dubovik et al. (2000), the uncertainty of the aerosol SSA at 440 nm retrieved from sun photometer measurements is 0.03 for $AOT_{440} > 0.2$, i.e. 3% of the median SSA value retrieved at our station in 2004-2010. The aerosol SSA at both wavelengths shows a significant decreasing trend with slopes equal to -0.6 ± 0.3 % $yr^{-1}$ and -0.8 ± 0.3 % $yr^{-1}$ at 440 and 675 nm, respectively, over periods where $AOT_{440} \geq 0.4$, i.e. about 25% of the time at IPR (not shown).

The trends over the 2004 – 2010 period in aerosol SSA monthly means calculated from aerosol scattering and absorption coefficients derived from measurements performed at ground level are almost identical to the trends in SSA data derived from sun photometer measurements, which are representative for ~1 to several km around the measurement site, and for the whole atmospheric column.

### 3.3. Origin and impact of the observed changes in aerosol characteristics

As indicated by the regressions in Figure 7a and 7b, $PM_{2.5}$ mass concentrations and aerosol scattering coefficients at 550 nm on the one hand, and EC mass concentrations and aerosol absorption coefficients at 520 nm on the other hand, are related to each other. Therefore, an increase of the EC contribution to $PM_{2.5}$ would be a straightforward explanation for the decrease of the aerosol single scattering albedo. Indeed, particles between 100 and 600 nm in diameter are the main contributors to both the scattering and absorption coefficients and $PM_{2.5}$ mass concentration at IPR. Such an increase in the $EC/PM_{2.5}$ ratio was actually observed over the 2000 – 2006 period, but no more since then. Changes in the EC content of $PM_{2.5}$ alone cannot therefore explain the trend observed in the aerosol SSA from 2004 to 2010.

It is apparent from Fig. 7b that the ratio absorption coefficient / EC concentration increased between 2005 and 2010, especially for the largest values, which in IPR are observed during cold months. This is confirmed by the significant increase in this ratio over the 2005 – 2010 period (+7 ± 1 % $yr^{-1}$, Fig. 8). This might be due to increasing concentrations of other light absorbing substances like brown carbon (detected as OC) during cold months over this period, during which wood burning for domestic heating was more and more used in Northern Italy (EDGAR data base).

Haywood and Shine (1995) and Chylek and Wong (1995) used Eq. 2 to assess the aerosol direct radiative forcing at the top of the atmosphere $F_a$:

$$F_a = -b\, F_T\, T^2\, (1-A_C)\, [\omega\, \beta_a (1-R_S)^2 - 2(1-\omega) R_S]\, \delta_a \qquad (2)$$

where $F_T$ is the solar constant (1366 W $m^{-2}$), $b$ is the fraction of daylight, $T$ is the transmissivity of the aerosol-free atmosphere (0.76), $A_C$ is the cloud cover, $\omega$ and $\beta_a$ the aerosol single scattering albedo and average upscatter fraction, respectively, $R_S$ the ground surface albedo, and $\delta_a$ the AOT (all dimensionless). We estimated the change in the aerosol direct radiative forcing at 550 nm for clear sky ($A_C = 0$) with a constant surface albedo $R_S = 0.175$ (as obtained from MODIS measurements at 550 nm). The

AOT at 550 nm was interpolated from the AOT measured by the sun photometer at 440 and 675 nm, and the Ångström equation (see e.g. Schuster et al, 2006, and references therein). The aerosol single scattering albedo and backscatter ratio in the mixed boundary layer (MBL) were calculated using monthly diurnal cycles of RH in the MBL as derived from 1 year of vertical profiles obtained from radiosondes launched from Milan – Linate airport (about 70 km SW of IPR) from October 2004, and the hygroscopic enhancement factors established in Adam et al., 2012. Figure 9 shows that the aerosol direct radiative forcing remained negative but decreased (in absolute value) over the 2004 -2010 periods by 0.9 ± 0.2 W $m^{-2}$ $yr^{-1}$. If the aerosol AOT had been constant (and equal to the mean value observe in 2005), the annual increment in direct aerosol forcing due to the decrease in aerosol SSA would have been +0.3 ± 0.1 W $m^{-2}$ $yr^{-1}$ only. In contrast, if the aerosol SSA had remained equal to its mean 2005 value, the observed change in the aerosol direct climate forcing due to the decrease in the AOT would have reached +0.8 ± 0.2 W $m^{-2}$ $yr^{-1}$. As changes in the aerosol backscatter ratio did not show any significant trend, they did not lead to any significant trend in the direct radiative forcing either. The decrease of the aerosol direct cooling effect calculated for IPR's area is therefore mainly due to the change in the aerosol AOT, and marginally amplified by the decrease in the aerosol SSA.

## 4- Conclusions

In the Po Valley (Northern Italy), where atmospheric pollution levels are extraordinary high because of large emissions and poor vertical and pollutant horizontal dispersions, particle concentrations decreased over the last decade, while European directives and other international protocols aiming to reduce people exposure to particulate pollution were implemented. Actually, at the regional background station IPR (NW of the Po Valley), not only has $PM_{2.5}$ mass concentrations at ground level decreased since 2004, but the aerosol optical thickness for visible light too. And whereas the decrease of $PM_{2.5}$ may be expected to be beneficial for health, the reduction of sunlight dimming by aerosols contributes to climate warming.

The aerosol direct radiative forcing does not however depend on the aerosol optical depth only, but also on the aerosol upscatter fraction and single scattering albedo. We did not observe any significant trend in the aerosol backscatter ratio. In contrast the aerosol single scattering albedo significantly decreased by about -0.7 ± 0.3 % $yr^{-1}$ in

the visible range over 2004 – 2010. This decrease in SSA cannot be explained from the measurements of EC and $PM_{2.5}$ concentrations alone, since no constant reduction of the EC / $PM_{2.5}$ ratio was observed over this period. An increase in the contribution of light absorbing organic matter to light absorption during cold months could be an explanation for the decrease in SSA.

Based on a 1-D approximated formula, we estimated that the cooling effect of the aerosol at IPR decreased by $0.9 \pm 0.2$ W $m^{-2}$ $yr^{-1}$ over this period, primarily due to the reduction in AOT, and secondly (~15%) due to the decrease in aerosol SSA.

It would be worth applying the methodology we presented at all sites where long-term measurements of the aerosol scattering, backscattering, and absorption coefficients (and also aerosol hygroscopicity data) are available. Recent developments in aerosol monitoring networks, data quality control and data management are making it possible for a larger and larger number of sites across the world. The results of such a study would tell us about the impact of current policies on the direct radiative forcing by aerosols. In areas where air pollution policies that target human health and ecosystem protection also lead to a reduction in AOT, the cooling effect of aerosols decreases. It decreases even more where air pollution abatement measures bring about a diminution in the aerosol SSA. With this information, it would then be possible to estimate how much radiative forcing could be "saved" by changing the SSA of pollution aerosols, i.e. by conceiving and implementing policies to mitigate the emission of light absorbing particles (e.g. soot), whether AOT decreases or not. Furthermore, since sufficient evidence exists of relationship between "black carbon" concentrations and short- and long-term health effects (Janssen et al., 2012), introducing limit values for "black carbon equivalent" or EC concentration in ambient air would be a win-win measure for both air quality enhancement and fast climate change mitigation.

## 5- References


Adam, M., J. P. Putaud, S. Martins dos Santos, A. Dell'Acqua, and C. Gruening, Aerosol hygroscopicity at a regional background site (Ispra) in Northern Italy, *Atmos. Chem. Phys.*, 12, 5703–5717, 2012

Anderson, T. L. and Ogren, J. A.: Determining Aerosol Radiative Properties Using the TSI 3563 Integrating Nephelometer, *Aerosol Sci. Tech.*, 29, 57–69, 1998.

Barnaba, F., Putaud, J. P., Gruening, C., Dell'Acqua, A., and Dos Santos, S.: Annual cycle in co-located in situ, total-column, and height-resolved aerosol observations in the Po Valley (Italy): Implications for ground-level particulate matter mass

concentration estimation from remote sensing, *J. Geophys. Res.*, 115, D19209, doi:10.1029/2009JD013002, 2010.

Begum B.A., Biswas S.K., Hopke P.K., Assessment of trends and present ambient concentrations of PM2.2 and PM10 in Dhaka, Bangladesh,. *Air Qual Atmos Health* 1:125–133, doi: 10.1007/s11869-008-0018-7, 2008

Cavalli F, Putaud J.P., Viana M., Yttri K., Genberg J. Toward a Standardised Thermal-Optical Protocol for Measuring Atmospheric Organic and Elemental Carbon: The EUSAAR Protocol,. *Atmos. Meas. Tech*.3 (1); 79-89, 2010.

Chen, L., G. Y. Shi, S. G. Qin, S. Yang, and P. Zhang: Direct radiative forcing of anthropogenic aerosols over oceans from satellite observations. *Adv. Atmos. Sci.*, 28, 973–984, doi: 10.1007/s00376-010-9210-4, 2011.

Chylek, P., and J. Wong, Effect of absorbing aerosol on global radiation budget, *Geophys. Res. Lett.*, 22, 929– 931, 1995.

Collaud Coen, M., Andrews, E., Asmi, A., Baltensperger, U., Bukowiecki, N., Day, D., Fiebig, M., Fjaeraa, A., Flentje, H., Hyv¨arinen, A., Jefferson, A., Jenning, S. G., Kouvarakis, G., Lihavainen, H., Lund Myhre, C. L., Malm, W. C., Mihapopoulos, N., Molenar, J. V., O'Dowd, C., Ogren, J., Schichtel, B. A., Sheridan, P., Virkkula, A., Weingartner, E., Weller, R., and Laj, P.: Aerosol decadal trends – Part 1: *In-situ* optical measurements at GAW and IMPROVE stations, *Atmos. Chem. Phys.*, 13, 869–894, doi:10.5194/acp-13-869-2013, 2013.

Dubovik, O., A. Smirnov, B. N. Holben, M. D. King, Y. J. Kaufman, T. F. Eck and I. Slutsker, Accuracy assessments of aerosol optical properties retrieved from AERONET Sun and sky-radiance measurements, *J. Geophys. Res.*, 105, (D8), 9791-9806, 2000.

EDGAR database, http://edgar.jrc.ec.europa.eu/overview.php?v=42

Haywood, J. M., and K. P. Shine: The effect of anthropogenic sulfate and soot aerosol on the clear sky planetary radiation budget. *Geophys. Res. Lett.*, 22,(5), 603-606, 1995.

Intergovernmental Panel on Climate Change (IPCC): Climate Change 2007: The Physical Science Basis, Contribution of Working Group I to the Fourth Assessment Report of the Intergovernmental Panel on Climate Change, edited by: Solomon, S., Qin, D., Manning, M., Chen, Z., Marquis, M., Averyt, K. B., Tignor, M., and Miller, H. L., Cambridge University Press, Cambridge, United Kingdom and New York, NY, USA, 2007.

Janssen, N.A.H., M.E. Gerlofs-Nijland, T. Lanki, R. O Salonen, F. Cassee, G. Hoek, P. Fischer, B. Brunekreef, M. Krzyzanowski, Health effects of black carbon, WHO Report, ISBN: 978 92 890 0265 3, Copenhagen, 2012.

Kloster, S., F. Dentener, J. Feichter, F. Raes, U. Lohmann, E. Roeckner, I Fischer-Bruns, A GCM study of future climate response to aerosol pollution reductions, *Clim Dyn.* 34:1177–1194, 2010

Müller, T., J. S. Henzing, G. de Leeuw, A.Wiedensohler, A. Alastuey, H. Angelov, M. Bizjak, M. Collaud Coen, J. E. Engström, C. Gruening, R. Hillamo, A. Hoffer, K. Imre, P. Ivanow, G. Jennings, J. Y. Sun, N. Kalivitis, H. Karlsson, M. Komppula, P. Laj, S.-M. Li, C. Lunder, A. Marinoni, S. Martins dos Santos, M. Moerman, A. Nowak, J. A. Ogren, A. Petzold, J. M. Pichon, S. Rodriquez, S. Sharma, P. J.

Sheridan, K. Teinilä, T. Tuch, M. Viana, A. Virkkula, E.Weingartner, R. Wilhelm, and Y. Q. Wang, Characterization and intercomparison of aerosol absorption photometers: result of two intercomparison workshops, *Atmos. Meas. Tech.*, 4, 245–268, 2011.

Murphy, D. M., Chow, J. C., Leibensperger, E. M., Malm, W.C., Pitchford, M., Schichtel, B. A., Watson, J. G., and White, W. H.: Decreases in elemental carbon and fine particle mass in the United States, *Atmos. Chem. Phys.*, 11, 4679–4686, doi:10.5194/acp-11-4679-2011, 2011.

Oh, H.-R., C.-H. Ho, and Y.-S. Choi: Comments on "direct radiative forcing of anthropogenic aerosols over oceans from satellite observation". *Adv. Atmos. Sci.,* 30(1), 10–14, doi: 10.1007/s00376-012-1218-5, 2013.

Putaud, J.P., *Interactive comment on* "Aerosol hygroscopicity at Ispra EMEP-GAW station" *by* Adam, M., Putaud, J. P., Martins dos Santos, S., Dell'Acqua, A., and Gruening, C, 2012, *Atmos. Chem. Phys. Discuss.*, 12, C1316–C1322, 2012.

Schuster, G.L., Dubovik, O., Holben, B.N., Ångström exponent and bimodal aerosol size distributions. *J. Geophys. Res.* 111, D07207, doi:10.1029/2005JD006328, 2006.

Shaw, R.G., and J.R. Etterson, Rapid climate change and the rate of adaptation: insight from experimental quantitative genetics, *New Phytologist* 195: 752–765, doi: 10.1111/j.1469-8137.2012.04230.x, 2012.

Tørseth, K., Aas, W., Breivik, K., Fjæraa, A. M., Fiebig, M., Hjellbrekke, A. G., Lund Myhre, C., Solberg, S., and Yttri,, K. E.: Introduction to the European Monitoring and Evaluation Programme (EMEP) and observed atmospheric composition change during 1972–2009, *Atmos. Chem. Phys.*, 12, 5447–5481, doi:10.5194/acp-12-5447-2012, 2012.

van Donkelaar, A., Randall, M., Brauer, M., Kahn, R., Levy, R., Verduzco, C., and Villeneuve, P.J. Global estimates of exposure to fine particulate matter concentrations from satellite-based aerosol optical depth. *Environ. Health Perspect.* 118, 847–855, http://dx.doi.org/10.1289/ehp.0901623, 2010.

Weatherhead, E. C., Reinsel, G. C., Tiao, G. C., Meng, X.-L., Choi, D., Cheang, W.-K., Keller, T., DeLuisi, J., Wuebbles, D. J., Kerr, J. B., Miller, A. J., Oltmans, S. J., and Frederick, J. E.: Factors affecting the detection of trends: Statistical considerations and applications to environmental data, *J. Geophys. Res.*, 103, 17149–17161, doi:10.1029/98JD00995, 1998.

Weingartner, E., Saatho, H., Schnaiter, M., Streit, N., Bitnar, B., and Baltensperger, U.: Absorption of light by soot particles: determination of the absorption coefficient by means of aethalometers, *J. Aerosol Sci.*, 34, 1445–1463, 2003.

WHO Fact sheet N°313, http://www.who.int/mediacentre/factsheets/fs313/en/ (last access: 27 March 2014), 2014.

## 6- Acknowledgements

This study was partially supported by the European research infrastructure projects EUSAAR (FP6-026140), and ACTRIS (FP7-262254). We thank all our colleagues in EUSAAR and ACTRIS for their fruitful collaboration during the last 8 years, M. Collaud Coen for her precious advice, F. Dentener and J. Ogren for their comments to

an earlier draft that greatly improved this manuscript, and J. Wilson and two anonymous referees for their comments to the current version.

414 Table 1: slope, standard error of the slope, and trends of variables observed at IPR, or
415 calculated from observations performed at IPR (2004 – 2010).

| variable | slope | standard error | trend |
|---|---|---|---|
| log($PM_{2.5}$, μg $m^{-3}$) | -3.3 % $yr^{-1}$ | 0.4 % $yr^{-1}$ | negative |
| log(aerosol scattering at 550 nm, $km^{-1}$) | -2.8 % $yr^{-1}$ | 0.5 % $yr^{-1}$ | negative |
| log(aerosol absorption at 550 nm, $km^{-1}$) | -1.1 % $yr^{-1}$ | 0.3 % $yr^{-1}$ | negative |
| log(aerosol optical thickness at 440 nm) | -4.0 % $yr^{-1}$ | 1.8 % $yr^{-1}$ | negative |
| log(aerosol optical thickness at 675 nm) | -2.5 % $yr^{-1}$ | 1.3 % $yr^{-1}$ | only just significant |
| log(aerosol absorption optical thickness at 440 nm) | +1.0 % $yr^{-1}$ | 1.0 % $yr^{-1}$ | not significant |
| log(aerosol absorption optical thickness at 675 nm) | +1.2 % $yr^{-1}$ | 0.9% $yr^{-1}$ | not significant |
| aerosol backscatter ratio at 520 nm | -0.1 % $yr^{-1}$ | 0.3% $yr^{-1}$ | not significant |
| aerosol scattering Ångström exponent | +0.1 % $yr^{-1}$ | 0.4% $yr^{-1}$ | not significant |
| aerosol single scattering albedo from *in-situ* measurements, 550 nm, 0% RH | -0.6 % $yr^{-1}$ | 0.2 % $yr^{-1}$ | negative |
| aerosol single scattering albedo at 440 nm from sun photometer measurements | -0.6 % $yr^{-1}$ | 0.3 % $yr^{-1}$ | negative |
| aerosol single scattering albedo at 675 nm from sun photometer measurements | -0.8 % $yr^{-1}$ | 0.3 % $yr^{-1}$ | negative |
| estimated direct aerosol radiative forcing (green light) | -(-0.9) W $m^{-2}$ $yr^{-1}$ | 0.2 W $m^{-2}$ $yr^{-1}$ | positive |

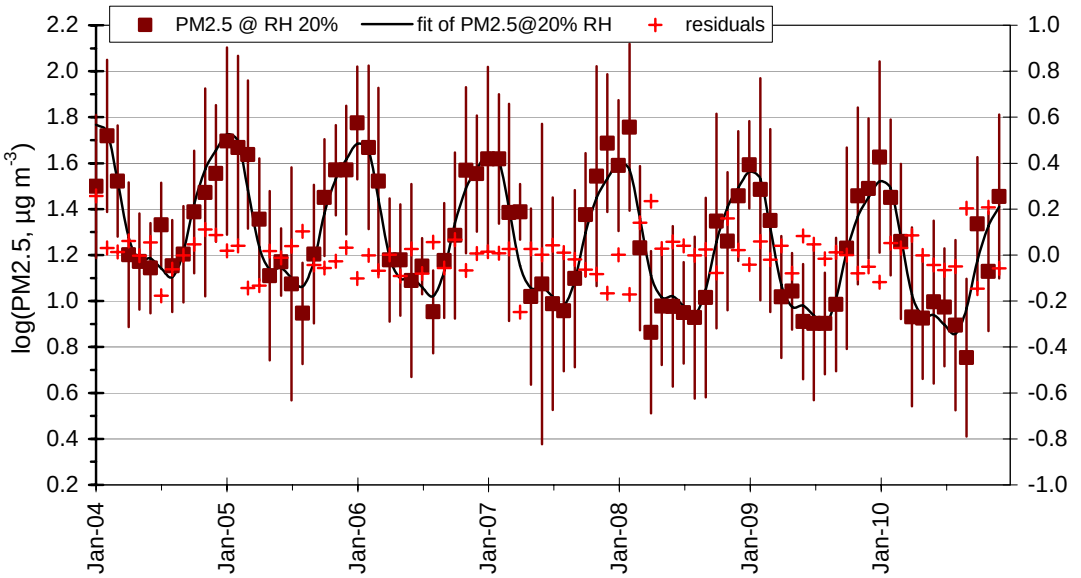


Fig. 1: variations in $PM_{2.5}$ at IPR: logarithm of the monthly mean values (squares), least mean square fit (line), and residuals (crosses, right axis). Error bars show the standard deviation of the log of the monthly averages.

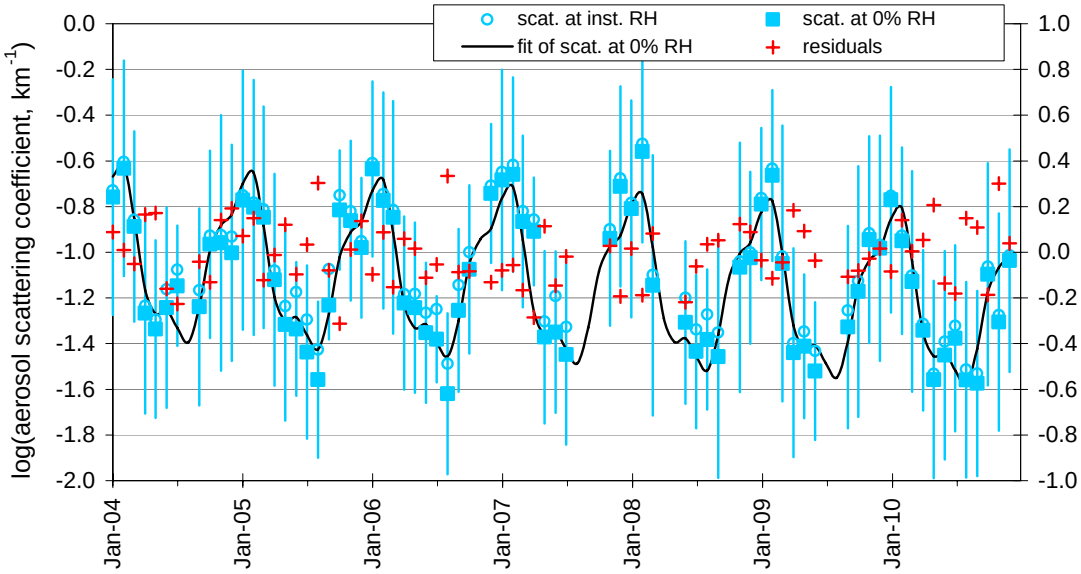


Fig. 2: variations in the aerosol scattering coefficient at 550 nm at IPR: logarithm of the monthly mean values at instrumental RH (open circles), at 0% RH (squares), least mean square fit of the logarithm of the monthly mean values at 0% RH (line), and residuals (crosses, right axis). Error bars show the standard deviation of the log of the monthly mean values at 0% RH.

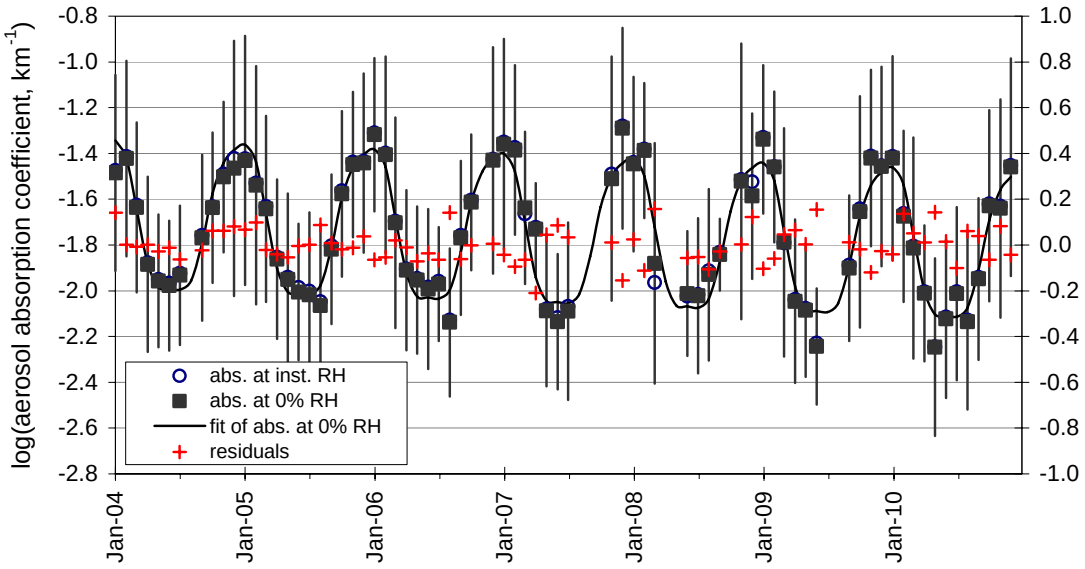


Fig 3: variations in the aerosol absorption coefficient at 520 nm at IPR: logarithm of the monthly mean values at instrumental RH (open circles), at 0% RH (squares), least mean square fit of the logarithm of the monthly mean values at 0% RH (line), and residuals (crosses, right axis). Error bars show the standard deviation of the log of the monthly mean values at 0% RH.

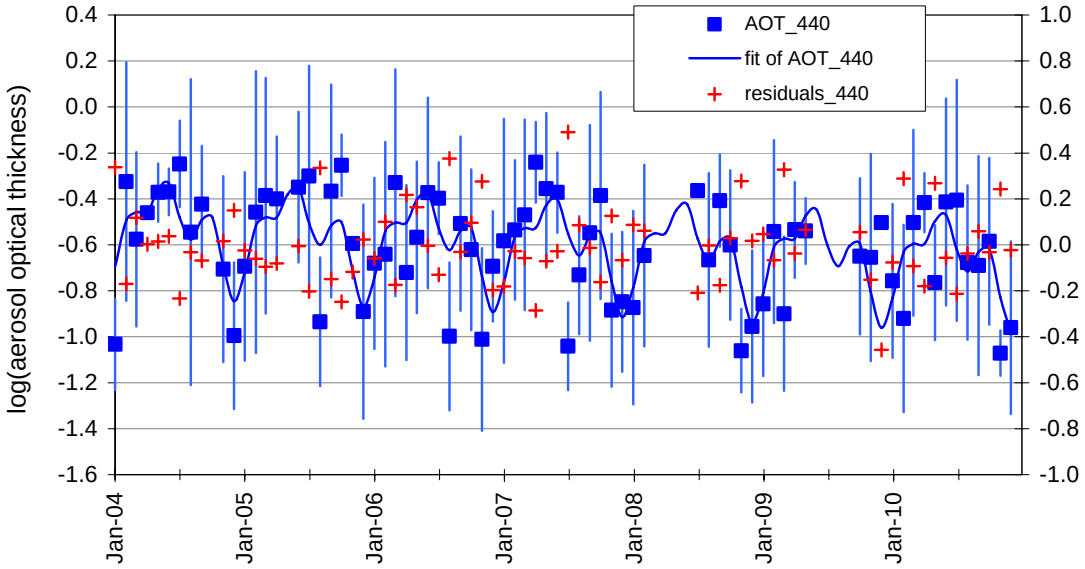


Fig 4: variations in the aerosol optical thickness at 440 nm at IPR: logarithm of the monthly mean values (squares), least mean square fit of the logarithm of the monthly mean values, and residuals (crosses, right axis). Error bars show the standard deviation of the log of the monthly averages.

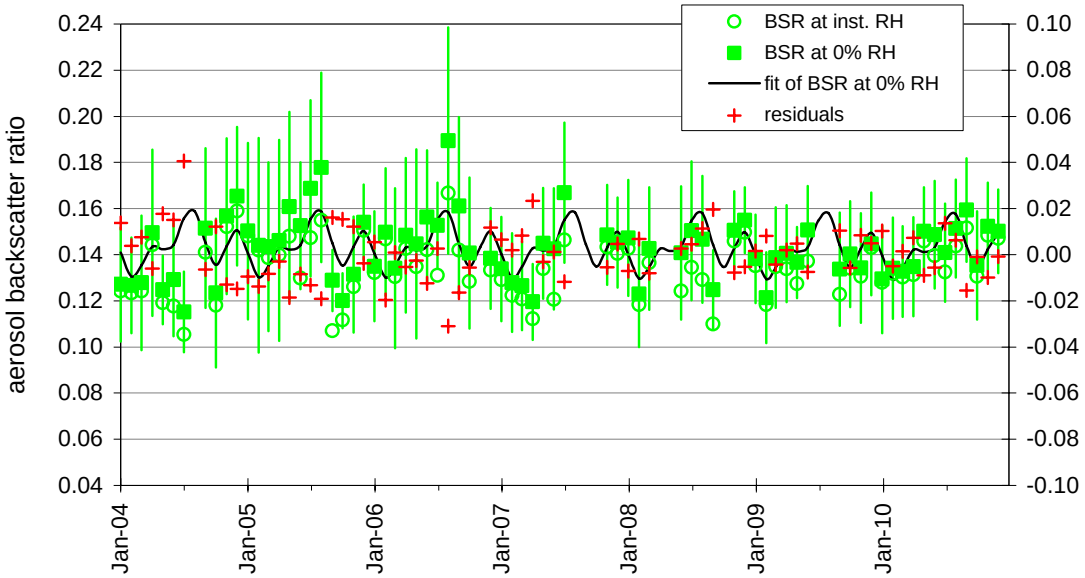


441

442 Fig. 5: variations in the aerosol backscatter ratio at 550 nm at IPR: monthly mean
443 values at instrumental RH (open circles), at 0% RH (squares), least mean square fit of
444 the monthly mean values at 0% RH (line), and residuals (crosses, right axis). Error
445 bars show the standard deviation of the monthly mean values at 0% RH.

446

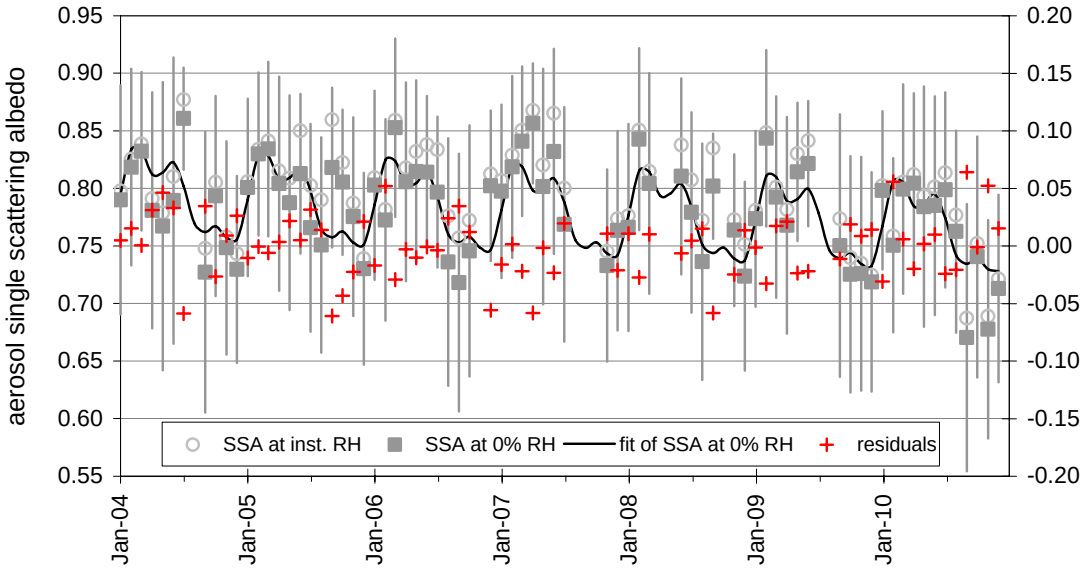


447

448 Fig. 6: variations in the aerosol single scattering albedo at 550 nm at IPR: monthly
449 mean values at instrumental RH (open circles), at 0% RH (squares), least mean square
450 fit of the monthly mean values at 0% RH (line), and residuals (crosses, right axis).
451 Error bars show the standard deviation of the monthly mean values at 0% RH.

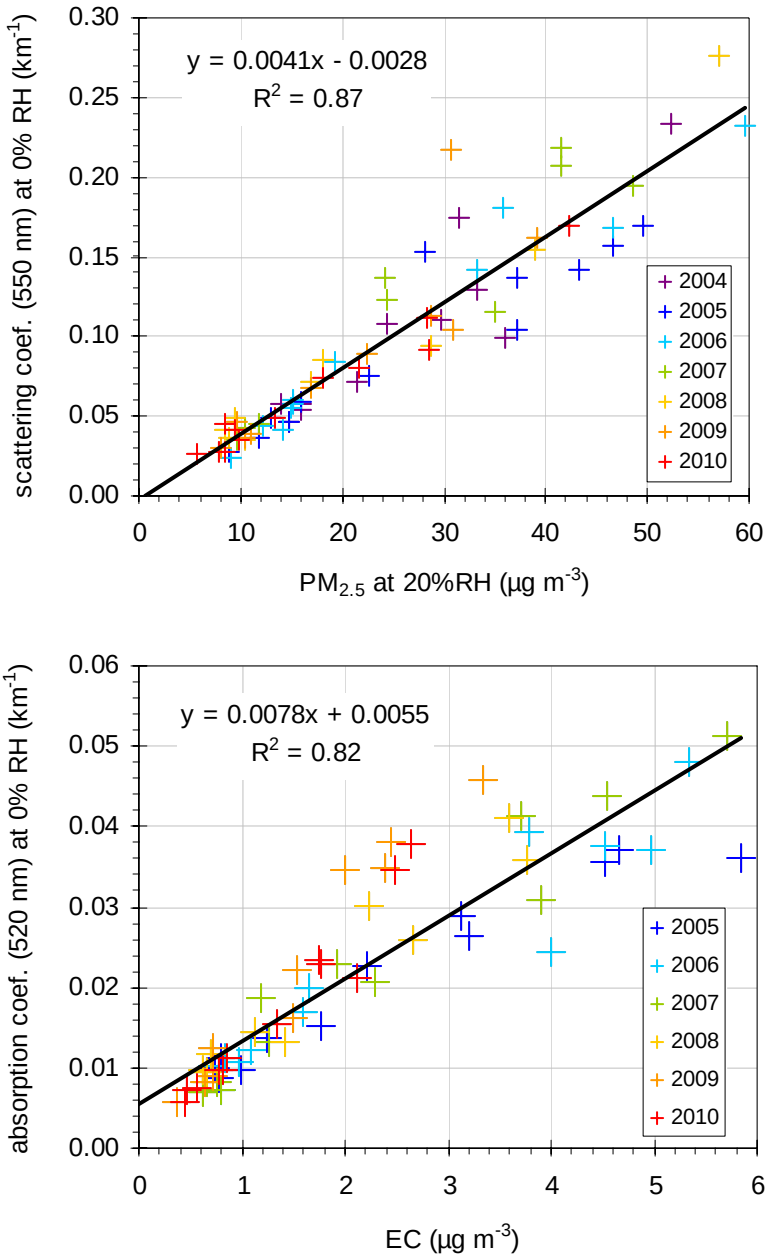


452

453 Fig. 7: regressions between monthly averages of (a) the aerosol scattering coefficient
454 and $PM_{2.5}$ mass concentration, and (b) the aerosol absorption coefficient and EC mass
455 concentration.

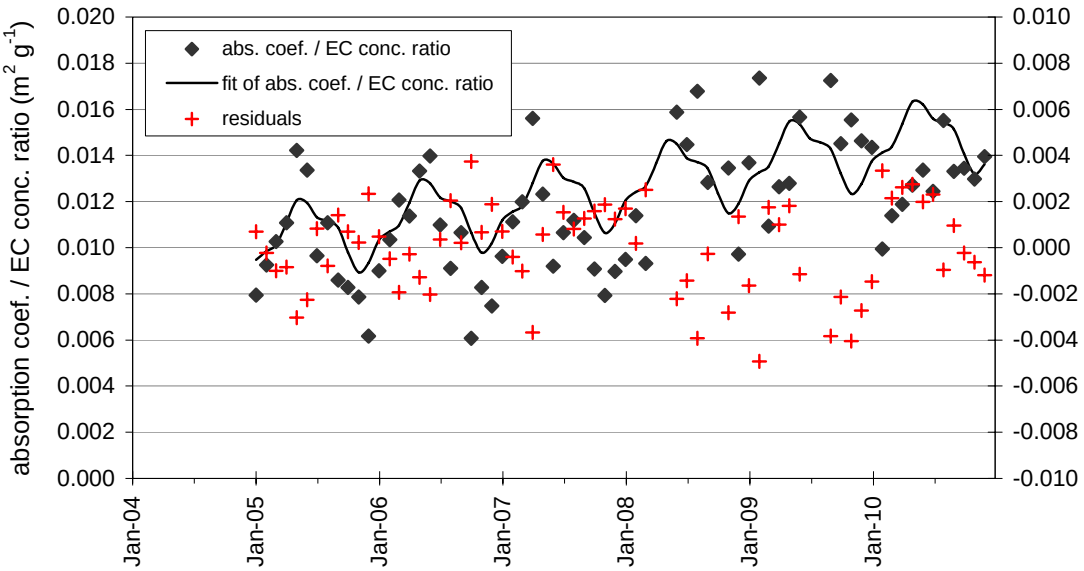


Fig. 8: variations in the aerosol absorption coefficient at 520 nm at 0% RH over EC concentration ratio at IPR: monthly mean values (diamonds), least mean square fit of the monthly mean values (line), and residuals (crosses).

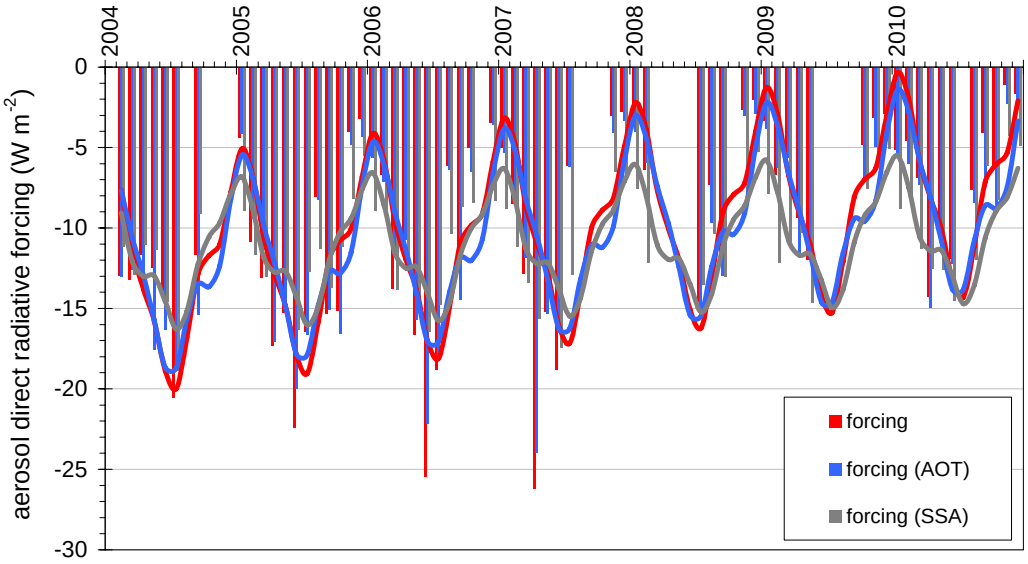


Fig. 9: estimates of the direct aerosol radiative forcing at 550 nm (red bars). Blue bars represent the change in aerosol forcing due to variations in AOT, and grey bars the change aerosol forcing due to variations in SSA. Corresponding lines represent the least mean square fits.